PHYSICAL REVIEW B VOLUME 51, NUMBER 15 15 APRIL 1995-I

Hydrogen interactions with cavities in helium-implanted germanium

S. M. Myers, H. J. Stein, and D. M. Follstaedt
Sandia National Laboratories, Albuquerque, New Mexico 87185-1056
(Received 16 November 1994)

The interactions of hydrogen with cavities in Ge were investigated and used to determine the binding energy of H at the Ge surface. Cavities were formed by He ion implantation and annealing, and their microstructure was characterized by transmission-electron microscopy. Hydrogen was then introduced by ion implantation, and during subsequent heating the bonding and eventual release of the H were monitored using Fourier-transform infrared spectroscopy and nuclear-reaction analysis. Analysis of the resulting data yielded a dissociation energy of 1.9 ± 0.2 eV for the Ge-H surface-monohydride bond. This implies that H_2 gas, with a binding energy of 2.26 eV per atom, is energetically preferred to the adsorbed state on Ge, in contrast to the situation for the Si surface.

I. INTRODUCTION

Hydrogen adsorption on the surfaces of Si and Ge has been extensively investigated, in significant part because of its technologically important passivating effects[1] and its strong influence on the chemical vapor deposition of Si-Ge alloys from hydrogenated reactants.[2] Considerable progress has been made in determining the structural arrangements of H on the (111) and (100) surfaces of both Si and Ge. Of particular relevance to the present discussion are the most strongly bound configurations, which are monohydride states with a semiconductor surface atom bonded to a single H atom and to three other semiconductor atoms.[1,3–5] The activation energy for recombinative H_2 desorption has been extensively measured for Si (see, e.g., Refs. 6–8), with data also being available for Ge.[9,10] The strengths of the Si-H and Ge-H surface bonds, however, have not been determined from ultrahigh-vacuum (UHV) experiments performed on external surfaces. This deficiency has two origins. First, the measured activation energy for desorption, E_D, does not by itself yield the surface-bond dissociation energy E_B. One has instead the relation

$$E_D = 2E_B - E_R + E_A , \quad (1)$$

where $E_R = 4.52$ eV is the energy released by H_2 formation from two gaseous H atoms, and E_A is the unmeasured activation energy for dissociative H_2 adsorption. The second cause of the deficiency is that the activation barrier for H_2 adsorption is sufficiently large to make this process difficult to observe on bare surfaces under UHV conditions, which is the principal reason that E_A has not been measured. Moreover, the same adsorption barrier has prevented observation of thermodynamic equilibrium between the bare external surfaces and H_2 gas, thereby precluding another conceivable approach to the determination of the surface-bond energy.

In previous experiments performed on Si, we circumvented the above difficulties by investigating the interaction of H with the internal surfaces of cavities.[11–13] These studies employed nuclear-reaction depth profiling of the H and Fourier-transform infrared (FTIR) spectroscopy of its bonded states. The cavities were formed by ion implanting He and then vacuum annealing, resulting in faceted voids from which the He had diffused. The interactions of H with the internal surfaces were then examined in two types of experiments to extract the Si-H surface-bond dissociation energy. In one of these, H that was initially bonded to the internal surfaces underwent thermal release during temperature ramping.[11] In this situation, the release of the H was controlled by its promotion from internal adsorption to solution and by its subsequent diffusion to the surface, rather than by the complicated recombinative desorption that governs release from external surfaces. As a result, the Si-H bond energy could be extracted unambiguously, and was determined to be 2.5 ± 0.2 eV. In the second type of experiment, the H population of internal-surface sites was measured under conditions of thermodynamic equilibrium with external H_2 gas, the interaction between the gas and the internal surfaces occurring by H diffusion.[12] Equilibrium was achieved despite the activation barrier to adsorption by using gas pressures up to 1 atm in conjunction with relatively high temperatures, a procedure that would be difficult with external UHV surfaces. It was thereby deduced that the Si-H surface binding energy is 2.67 ± 0.1 eV, consistent with the value from temperature ramping.

In this paper we discuss analogous ion-beam studies of H interactions with cavities in Ge, the primary objective again being to determine the bond dissociation energy for the surface-monohydride state. The determination of E_B for Ge proved to be more complicated than for Si, primarily because the H_2 gas phase is energetically preferred to adsorption on Ge. Because of this, the H associated with cavities existed mostly as H_2 within the void, with only a small fraction being bound as Ge-H on the walls. Nevertheless, FTIR spectroscopy permitted the adsorbed component to be semiquantitatively evaluated, and this provided a basis for evaluating the Ge-H bond energy.

0163-1829/95/51(15)/9742(10)/$06.00 ©1995 The American Physical Society

II. EXPERIMENTAL PROCEDURES

Germanium samples were prepared from material having a room-temperature resistivity of $>40\,\Omega\,\mathrm{cm}$. The specimens used for nuclear-reaction analysis had dimensions of $12.5\times12.5\times0.25$ mm^3 with one polished (111) face. Samples employed for FTIR spectroscopy were parallelepiped internal-reflection plates 10 mm in length and 0.5 mm thick with 45° entrance and exit faces, and the two large faces were of (111) orientation. Internal-reflection spectroscopy with this geometry increased the sensitivity to Ge-H centers by about 14 times relative to normal-incidence transmittance, and an additional factor of 2 was gained by introducing cavities on both sides of the plate. The cavities were formed by ion implanting He at room temperature to a dose of 1000 nm^{-2} using an energy of 50 keV, followed by annealing for 30 min at 973 K in a vacuum of approximately 3×10^{-5} Pa (2×10^{-7} Torr). The anneal served to induce outgassing of the He, enlarge the cavities, and remove ion-implantation damage. The resulting microstructure was characterized by cross-section transmission electron microscopy (TEM) of equivalently treated samples using an electron energy of 200 keV. Hydrogen was introduced into the specimens by room-temperature ion implantation at 28 keV, an energy chosen to produce approximate overlap with the cavity-containing layer. The H dose was 100 nm^{-2} in all cases except one, where the value was reduced to 10 H/nm^2.

We examined the behavior of H in these samples in two types of experiments. In one type, the temperature was ramped upward at 2 K/min in a turbomolecular-pumped vacuum of about 3×10^{-5} Pa, and the depth-integrated areal density of H remaining within the cavity layer was monitored *in situ* by nuclear-reaction analysis. The deuterium isotope (D) was employed, and it was detected using the ^{3}He-induced nuclear reaction D(^{3}He,p)^{4}He with an incident ^{3}He energy of 0.7 MeV, as discussed in detail elsewhere.[11] Because these temperature ramps extended to about 1100 K, it was important to achieve good thermal contact between the thermocouple temperature sensor and the Ge sample. To this end, we welded a chromel-alumel thermocouple bead to a Mo plate and then formed a reaction bond between the Mo plate and the back side of the Ge. The bond was formed by introducing a 15-μm foil of Al between the Ge and Mo and raising the temperature to 973 K for 30 min under vacuum. The implantation of He was carried out before bonding, and the bonding anneal then served to develop the cavity microstructure as discussed above. Implantation of D was carried out *in situ* just prior to temperature ramping.

The second type of experiment used FTIR spectroscopy to characterize the bonding states of the H during isochronal annealing sequences. The anneals were performed in flowing, high-purity N_2 gas; each anneal lasted for 30 min and was terminated by moving the quartz sample boat to a position outside of the high-temperature region of the furnace but still within the flowing N_2. Because a transfer of H from cavity-wall states to encapsulated H_2 gas within the cavities was believed to occur during cooling, the time-temperature profile of the sample boat was measured in detail; the temperature decayed nearly exponentially to 378 K with a $1/e$ time of 170 s. The Ge multiple-internal-reflection plates were implanted with He and H on both large faces, and the IR-absorption spectrum was measured at room temperature with a resolution of 2 cm^{-1}. The protium isotope (^{1}H) was used instead of D for FTIR spectroscopy because its vibration spectrum has a greater amplitude and appears at higher frequencies. Background subtraction was carried out using spectra from unimplanted samples.

III. RESULTS AND INTERPRETATION

A. Cavity microstructure from transmission electron microscopy

Figure 1 shows a cross-section TEM image of the cavities formed in Ge by implanting 1000 He/nm^2 at an energy of 50 keV, and then vacuum annealing for 30 min at 973 K. The depth distribution of the cavities conforms approximately to the depth profile of implanted He calculated using the Monte Carlo range code TRIM-90 (Ref. 14), which predicts an average projected range of 290 nm and a root-mean-square range spread of 110 nm. The cavity surfaces exhibit some well-resolved {111} facets in conjunction with apparently curved regions that presumably reflect higher step densities. A full characterization of the cavity faceting, including the detection of possible {100} and {110} faces, would necessitate observation at other orientations and is beyond the scope of this paper. Detailed analysis of Fig. 1 and similar micrographs yielded the following relevant properties: the average cavity diameter is 60 nm, the cavity surface area per unit sample area is 3.8 ± 1.0 nm^2/nm^2, and the cavity volume per unit sample area is 44 ± 11 nm^3/nm^2. The number of cavity-

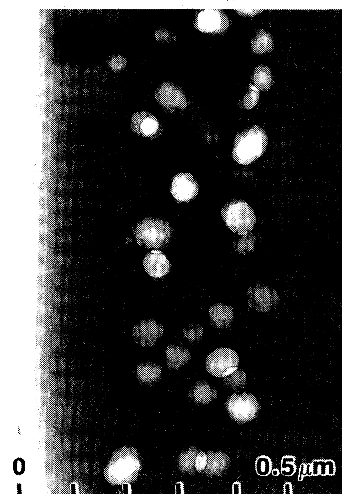

FIG. 1. Cross-section bright-field TEM micrograph of Ge that was ion implanted with 1000 He/nm^2 at 50 keV and then vacuum annealed for 30 min at 973 K. The orientation is $[11\bar{2}]$, and the imaging was performed at a slight underfocus to enhance the contrast of open volumes.

wall binding sites for H per unit sample area can be estimated from the wall surface area. In doing this we use the average of the H areal densities for the ideal saturated monohydrides on (111) and (100) Ge surfaces,[1,3–5] $(7.24+6.27)/2=6.76\ \text{nm}^{-2}$, giving 26 binding sites per nm^2 of sample area. A single spherical cavity of diameter 60 nm is estimated in similar fashion to contain 76 000 binding sites.

The anneal at 973 K is calculated to remove most of the He from the cavities by diffusion, leaving open volumes that can be regarded as empty insofar as H behavior is concerned. The He release rate is estimated by assuming an ideal-gas equation of state and using the reported diffusion coefficient and solid solubility of He in Ge.[15] The product of these two quantities is the permeability, and, at 973 K and 1-atm pressure, its value is calculated to be 0.26 atoms/nm/s. Therefore, at the instant when the pressure of He remaining within the cavities is 1 atm, the release flux is approximately equal to this permeability divided by the average depth of the cavities, or 9.0×10^{-4} atoms/nm^2/s. Moreover, at the same pressure and temperature, the areal density of gaseous He atoms contained within a cavity-volume areal density of 44 nm^3/nm^2 is 0.33 atoms/nm^2. Hence the time constant for exponential decay of the amount of retained He, applicable for pressures where the ideal-gas equation of state is obeyed, is (0.33 atoms/nm^2)/(9.0×10^{-4} atoms/nm^2/s) or about 6 min. This means that the 30-min anneal should reduce the amount of implanted He by a factor of approximately 150. Since this treatment underestimates the He chemical potential at higher densities, the amount of He actually released should be somewhat greater.

After the anneal at 973 K, which is 80% of the absolute melting temperature of Ge, residual defects from He implantation are believed to be inconsequential for the observed behavior of H. Indeed, various studies of damage annealing in both ion-implanted and fast-neutron-irradiated Ge show the recovery going to completion below 800 K.[16] Moreover, when one of the present He-implanted specimens was TEM imaged so as to enhance the strain contrast of dislocations, only a few were observed, all within the cavity layer and presumably stabilized by the cavities.

B. Hydrogen thermal release observed by nuclear-reaction analysis

Figure 2 shows data from three temperature-ramp experiments in which the retention of ion-implanted H was monitored by nuclear-reaction analysis. As discussed above, the D isotope was used, and was detected through the nuclear reaction $D(^3He,p)^4He$. The nominal implantation dose was 100 H/nm^2. Two of these experiments were performed on identically prepared samples that contained cavity layers like the one shown in Fig. 1, and the combined, redundant data are plotted as open circles. The data represented by triangles are from a third, control sample that was implanted with D but not with He to form cavities. The cavity-containing specimens are seen to retain essentially all of the H until a temperature

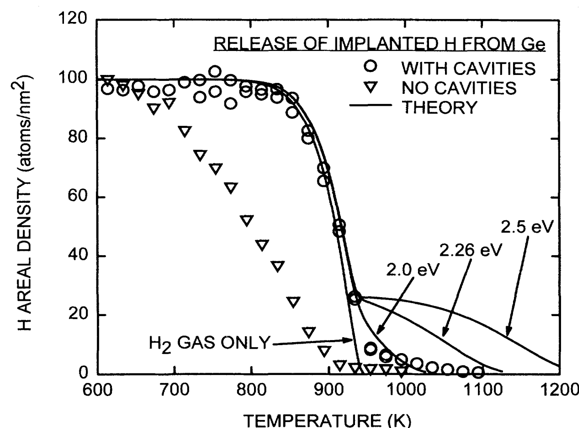

FIG. 2. Areal density of ion-implanted H remaining in Ge as a function of temperature during temperature ramping at 2 K/min. The depth-integrated areal density of H was measured by nuclear-reaction analysis.

of about 900 K, whereupon there is a single, sharply defined release stage. In the absence of cavities, H release begins at about 700 K and is nearly complete before the onset of the stage in the cavity-containing material. Our qualitative interpretation is that, in the absence of cavities, the H is initially trapped at a variety of defects produced during its implantation, and the release above 700 K is then due to a combination of detrapping and defect annihilation. The relatively abrupt stage at higher temperature in the presence of cavities is then believed to reflect binding of H to the cavities, and the mechanisms by which this occurs are the principal concern of the remainder of this paper. A simplifying factor in the release from cavities is that these entities can be regarded as static throughout the process, since microstructural evolution is insignificant below the temperature of the earlier, 973-K anneal that followed He implantation.

There are two plausible mechanisms for H binding at the cavities: chemisorption on the walls and formation of molecular gas within the open volumes. In order to interpret the observed thermal evolution we mathematically modeled these effects and the accompanying lattice diffusion, using a diffusion-reaction formalism that was discussed in detail elsewhere.[11] Briefly, in this formalism the changing depth distribution of the H is described by the diffusion equation, with source terms to take account of H transfer to and from bound states. One then has

$$[\partial/\partial t]C_s(x,t)=D_s[\partial^2/\partial x^2]C_s-\Sigma_i S_i(x,t) \tag{2}$$

and

$$[\partial/\partial t]C_i(x,t)=S_i(x,t)\ , \tag{3}$$

where C_s is the atomic fraction of mobile H in solution, D_s is the diffusion coefficient, S_i is the source term associated with bound state i, and C_i is the atomic fraction of H in this state. For static reversible traps such as surface chemisorption sites, which we index as $i=1$, the source term is given by

$$S_1(x,t)=4\pi N_h D_s[R_1/n_1]\{C_s(x,t)[A_1(x)-C_1(x,t)] - C_1\exp(-Q_1/kT)\} . \quad (4)$$

In Eq. (4), N_h is the atomic density of the host; R_1 is the effective capture radius for a discrete trapping entity such as a cavity; n_1 is the number of H attachment sites per trapping entity, being for a cavity the number of attachment sites on the wall; A_1 is the atomic concentration of the attachment sites; and Q_1 is the positive binding energy per H atom at the trap site expressed relative to the solution state. In the particular case of trapping at cavity-wall chemisorption sites, the quantity Q_1 is related to the Ge-H surface-bond dissociation energy E_B by

$$Q_1=E_B+E_S-E_R/2 , \quad (5)$$

where E_S is the energy per atom required to promote H from molecular gas to solution in Ge, and E_R is the dissociation energy of the H_2 molecule. The cavity-wall-trap concentration profile A_1 is taken to be a Gaussian function with the first and second moments of the calculated He implantation profile,[14] and an integrated area equal to the areal density of wall traps estimated from TEM.

At this point we consider more precisely what is meant by the various energies in Eqs. (4) and (5). Rigorously, Q_1 in Eq. (4) represents a change in thermodynamic free energy when a H atom moves from internal chemisorption to solution at temperature T; this quantity is given by $\Delta H_1 - T\Delta S_1$ where ΔH_1 is the change in enthalpy and ΔS_1 is the change in the nonconfigurational, vibrational part of the entropy. Since the conditions of our experiments permit multiple hops of a particular H atom between chemisorption and solution, leading to local equilibration before diffusion from the cavity layer, Q_1 and the value of E_B derived from it should include the effects of any changes in the internal surface that may arise from the removal of H, such as relaxation or reconstruction. Further, we assume that the vibrational entropies associated with surface Ge-H and with H in solution sites in the bulk lattice are sufficiently similar to neglect ΔS_1, thereby treating Q_1 simply as the binding enthalpy relative to solution. Some justification for this common approximation comes from theoretical work on H in Si, where vibrational modes for surface monohydrides are found to correspond closely in frequency with modes due to bond-center H in bulk solution.[17] Within the context of these definitions and assumptions, the quantities in Eq. (5) should be regarded as reaction enthalpies evaluated in the temperature range of the experiments. For simplicity, however, we equate $E_R/2$ to its zero-temperature value of 2.26 eV; this neglects a decrease with increasing temperature that amounts to only 0.08 eV at 500 K (Ref. 18), the approximate temperature where the relationship of Eq. (5) is actually used to determine E_B, as discussed in Sec. III C.

For H bound as a diatomic gas within the cavity open volume, which we index as $i=2$, one has

$$S_2(x,t)=4\pi N_h D_s[R_2/n_2]A_2(x) \times\{C_s(x,t)-C_{so}[F_2(C_2,A_2,T)]^{1/2} \times\exp(-Q_2/kT)\} , \quad (6)$$

where C_{so} is the solubility prefactor, F_2 is the fugacity of the gas, and Q_2 is the solubility activation energy. Here we take Q_2 to be equal to the solution enthalpy E_S, although the two quantities may in fact differ slightly. The fugacity, which equals pressure when the H_2 behaves as an ideal gas, is a function of the amount of H in the gas phase parametrized as C_2, the available cavity volume parametrized as A_2, and the temperature T. In treating this functional relationship we employed the Van der Waals equation of state with only the volume term, leading to the relation

$$F_2(C_2,A_2,T)=[kT/b][C_2/(A_2-C_2)] \times\exp[C_2/(A_2-C_2)] , \quad (7)$$

where b is the Van der Waals molecular volume. In Eqs. (6) and (7), n_2 and A_2 are both defined in terms of the number of H atoms that can exist as H_2 within the cavities in the limit where the volume per molecule approaches b. The quantity n_2 is then simply twice the volume per cavity divided by b. The profile $A_2(x)$ is again taken to be a Gaussian function with the first and second moments of the calculated He implantation profile, but the integrated area in this case is equal to twice the cavity volume per unit sample area divided by b. Finally, the boundary condition at the external sample surface during temperature ramping is taken to be $C_s(x\rightarrow 0,t)=0$, implying the absence of any significant barrier. This system of coupled equations is solved numerically to obtain C_s, C_1, and C_2 as functions of depth and time.

The above formalism was first used to model the temperature ramp experiment of Fig. 2 under the assumption that the H only formed H_2 gas within the cavities, as described by Eq. (6), there being no chemisorption on the cavity walls. This calculation was done with no free parameters, the various quantities in the equations being independently evaluated as specified in Table I. The results are given by the lowermost theoretical curve in Fig. 2. This restricted treatment is seen to provide a rather good description of the experimental data, both in the shape of the release stage and in its absolute position on the temperature scale. With regard to the shape, it is specifically noteworthy that both data and theory do not exhibit the pronounced sigmoidal character that is generally observed for release from traps; instead, the temperature derivative of the retained quantity continues to increase in magnitude with temperature until most of the H has escaped. The reason for this is that the release is occurring due to the dissipation of a precipitated second phase, namely H_2 gas, leading to a weaker dependence of the H chemical potential on retained quantity than one would have for release from static traps. This distinction may be seen by considering a state of local equilibrium where S_1 in Eq. (4) and S_2 in Eq. (6) are both equal to zero, giv-

TABLE I. Parameters used to model H behavior in cavity-containing Ge.

Parameter	Meaning	Value	Source
D_s	H diffusion coefficient	$(0.27\ \mathrm{mm^2/s})\exp(-0.377\ \mathrm{eV}/kT)$	Ref. 19
R_1	capture rad. for cav.-wall binding	30 nm	TEM
R_2	capture radius for H_2 in cavity	30 nm	TEM
n_1	no. wall binding sites per cavity	76 000	TEM, see text
$\Lambda_{\mathrm{Ge}\text{-}}$	no. wall bind. sites per sample area	26 $\mathrm{nm^{-2}}$	TEM, see text
Λ_V	cavity volume per sample area	44 $\mathrm{nm^3/nm^2}$	TEM
b	effective Van der Waals H_2 volume	0.028 $\mathrm{nm^3}$/molecule	Ref. 20
n_2	max. no. atoms in H_2 gas per cav.	8.1×10^6	2(cav. vol.)/b
$Q_2 \cong E_S$	H_2 bind. ener. per atom rel. to soln.	2.29 eV	Ref. 19
C_{so}	H solubility prefactor	0.23 atom fraction/$\mathrm{Pa^{1/2}}$	Ref. 19
$A_1(x)$	depth profile of cavity-wall sites	(0.0021 atom fraction) $\times\exp[-(x-290\ \mathrm{nm})^2/2/(110\ \mathrm{nm})^2]$	TEM, TRIM (Ref. 14)
$A_2(x)$	saturation depth profile of H in H_2	(0.26 atom fraction) $\times\exp[-(x-290\ \mathrm{nm})^2/2/(110\ \mathrm{nm})^2]$	TEM, TRIM (Ref. 14)
ν_D	desorption attempt frequency	$10^{16}\ \mathrm{s^{-1}}$	See text
E_D	desorption activation energy	1.82 eV	Ref. 10
E_R	H_2dissociation energy at 0 K	4.52 eV	

ing in the limit of small H content $C_s \propto C_1$ for traps and $C_s \propto C_2^{1/2}$ for the diatomic gas.

The above comparison between experiment and calculation suggests that the H within the cavity-containing Ge existed almost entirely as H_2 gas. This is in marked contrast to our findings for cavity-containing Si, where wall chemisorption dominated and there was significant H_2 formation only after the chemisorption sites were saturated; it implies that the relative stabilities of the gaseous and chemisorbed states are qualitatively different in Ge. This inference will be examined further in Sec. III C, where we present results from FTIR vibrational spectroscopy.

We now consider more quantitatively the implications of the temperature-ramp data for the strength of Ge-H surface bonds. This is done by introducing cavity-wall trapping into the modeling using Eqs. (4) and (5). We employ three trial values of the bond energy E_B: 2.5 eV, equal to the Si-H surface-bond energy extracted from similar experiments on Si; 2.26 eV, the dissociation energy per atom of the gaseous H_2 molecule at zero temperature; and 2.0 eV, which is just sufficient to have a noticeable influence on the calculated release curve. Other parameter values and their origins are given in Table I. The results of the three calculations are given by the correspondingly labeled curves in Fig. 2. These curves exhibit a pronounced high-temperature step associated with wall trapping that is not evident in the experimental data. From this disparity we infer that $E_B \lesssim 2.0$ eV. For a more precise determination of E_B we now consider the results from FTIR spectroscopy, which can specifically distinguish the internally chemisorbed component of the H.

C. Hydrogen states observed as a function of temperature by infrared spectroscopy

Figure 3 shows FTIR spectra from a cavity-containing Ge specimen during a sequence of isochronal anneals after implantation of 100 $^1\mathrm{H/nm^2}$ at room temperature. Figure 4 provides an expanded view of the spectra obtained from the samples annealed at more elevated temperatures. The He implantation and vacuum anneal to form the cavities were the same as those leading to Figs. 1 and 2, and the isochronal anneals after H injection were performed in flowing dry N_2 gas for 30 min each. Figure 5 presents parallel results from a specimen without cavities that was otherwise identically treated. We also obtained spectra from a cavity-containing sample in which the implanted H dose was reduced to 10 $\mathrm{nm^{-2}}$, and these data are shown in Fig. 6.

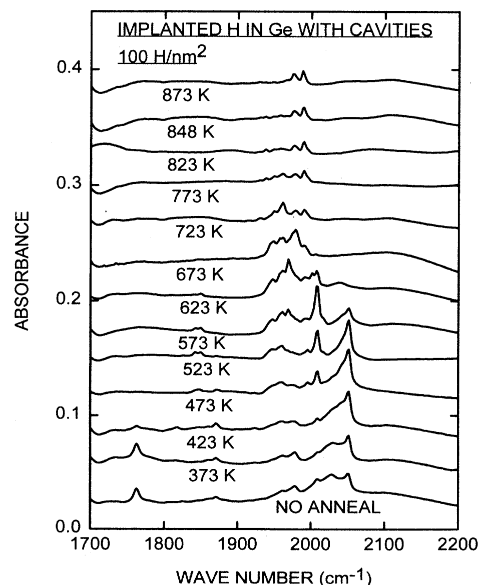

FIG. 3. Infrared-absorption spectra from ion-implanted H in cavity-containing Ge during isochronal annealing. The H dose is 100 $\mathrm{nm^{-2}}$.

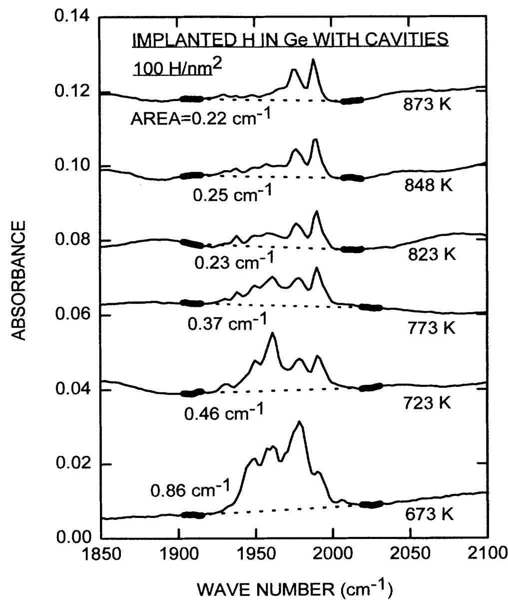

FIG. 4. Expanded view of IR-absorption spectra from ion-implanted H in cavity-containing Ge during isochronal annealing. The H dose is 100 nm^{-2}. The dashed lines are base lines used to integrate the area under the H-related region of the spectrum, and were obtained by least-squares fitting to the highlighted segments.

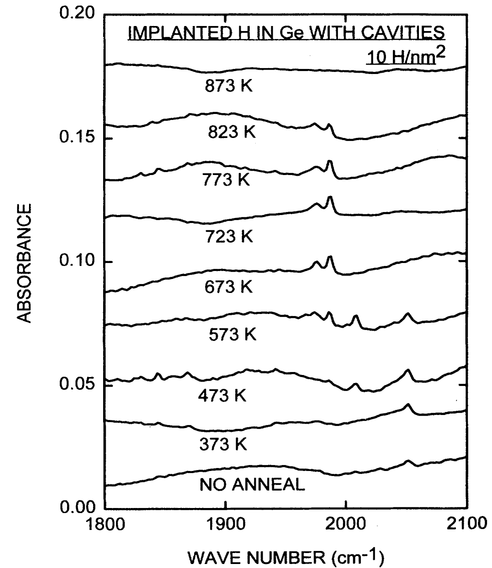

FIG. 6. Infrared-absorption spectra from a reduced dose of ion-implanted H in cavity-containing Ge during isochronal annealing. The H dose is 10 nm^{-2}.

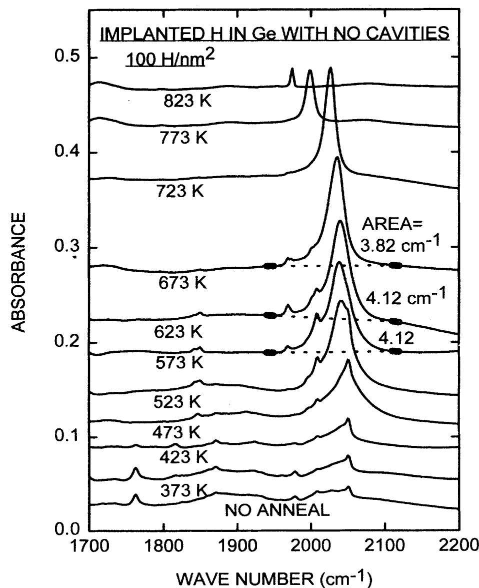

FIG. 5. Infrared-absorption spectra from ion-implanted H in Ge without cavities during isochronal annealing. The H dose is 100 nm^{-2}. The dashed lines are base lines used to integrate the area under the H-related region of the spectrum, and were obtained by least-squares fitting to the highlighted segments.

The two H-related spectra in Figs. 3 and 5 that were obtained before the H-implanted Ge was annealed, from samples respectively with and without cavities, span an extended frequency range and have several resolved peaks in common. These data qualitatively resemble spectral results from H-implanted Si that are much more extensive and have been theoretically treated,[21,22] and we propose that the same general interpretation applies here. It is that, during implantation, the H becomes trapped at a variety of defects arising from implantation displacement damage. The partitioning of the H among these defect traps at room temperature is largely opportunistic rather than reflecting relative thermal stabilities. For example, much of the implanted H is not associated with the available cavities, even though the annealing behavior discussed in Sec. III B and below indicates that this condition is the most stable one. The assignment of the numerous room-temperature spectral peaks to specific H-defect complexes is likely to prove complicated for Ge, as it was for Si, and since the matter is peripheral to the present paper it will not be addressed here.

As the anneal temperature rises, the IR spectrum from cavity-containing Ge becomes increasingly different from that measured in the absence of cavities. When cavities are present, the spectral yield increasingly shifts into the frequency range 1920–2000 cm^{-1}; at the most elevated temperatures, there are two prominent peaks at about 1976 and 1988 cm^{-1}, respectively, with lower-amplitude features extending downward in frequency. This conforms closely to spectra that were obtained in UHV studies of H on the external (111) and (100) surfaces of Ge

and were ascribed to surface-monohydride states.[23,24] In particular, exposure of the (111) surface to atomic H at 500 K was reported to produce a single sharp monohydride peak at 1971 cm^{-1}, whereas room-temperature exposure of the (100) surface produced prominent peaks at 1979 and 1991 cm^{-2} with weaker features extending downward to about 1925 cm^{-1}. A second noteworthy feature of the cavity-containing material is that the area under the spectrum decreases by several times as the temperature is increased to 723 K, despite the fact that the nuclear-reaction experiments discussed above and plotted in Fig. 2 indicate that essentially all of the H remains within the specimen until the temperature rises an additional 150 K. Between 773 and 873 K, there is relatively little change in the spectral area, as seen in Fig. 4. Our interpretation is that, as the temperature increases, the H progressively moves from defect traps to the cavities, where most of it forms H_2 gas within the voids and thereby ceases to absorb IR light. A small fraction adsorbs onto the internal surfaces of the cavities, however, and this component is responsible for the surfacelike spectrum with the two prominent peaks.

As the Ge not containing cavities is annealed at increasingly elevated temperatures, the IR spectrum first coalesces into a single prominent peak centered at about 2040 cm^{-1}, and then remains essentially static for a time. The peak then decays in the approximate temperature range 723–823 K, paralleling the reduction in total retained H observed by nuclear-reaction analysis and plotted in Fig. 2. During this decay the frequency shifts downward, reaching about 1974 cm^{-1} as the peak disappears. We hypothesize that the initial coalescence reflects the disappearance of the multiplicity of H-defect complexes present at room temperature in favor of a single, more thermally stable H-defect center; this center then dissociates at still higher temperatures, giving rise to the H release seen in Fig. 2. The structural identity of the latter center is uncertain at present, but the comparison of its Ge-H stretch vibrational frequency with those for GeH molecular species is nevertheless suggestive. In particular, the frequencies reported for GeH_2 and GeH_4, respectively, are 1887 and 2106 cm^{-1} (Ref. 25), and these lie on either side of the peak under consideration. This leads us tentatively to speculate that the H is bound to a vacancy complex with a local bonding configuration such that a Ge atom is attached to three H atoms and to one other Ge atom associated with the host matrix, $Ge—Ge\equiv H_3$. This higher-hydride condition develops because the number of vacancy complexes is insufficient to contain all of the H atoms in a monohydride state. During thermal release of the H, however, the bonding may revert to $Ge_2=Ge=H_2$ and then $Ge_3\equiv Ge—H$, causing the observed reduction in peak frequency.

We now return to the behavior of the H in cavity-containing material and consider its implications for the dissociation energy of the Ge-H surface monohydride bond. The most illuminating IR spectra in this regard are those in Fig. 4 obtained after annealing at 823, 848, and 873 K, where the spectrum has essentially stabilized and the release of H from the sample has not begun. These temperatures are also well above the range of H thermal desorption from external Ge surfaces, which occurs below 700 K even at ramp rates as high as $\sim 10^3$ K/min,[9,10] and consequently the chemisorbed monohydride on the cavity wall is expected to come into equilibrium with the molecular gas within the cavity open volume. Hence the partitioning of H between these two states, as observed by FTIR spectroscopy and nuclear-reaction analysis, is indicative of relative energies. Qualitatively, the sequence of spectra in Fig. 3 coupled with the release data in Fig. 2 indicates that the amount of Ge-H is much smaller than the amount of H_2, suggesting that H_2 is the more stable state. We now proceed to develop this inference at a more quantitative level.

Our treatment of the interplay between surface Ge-H and H_2 gas will be presented in two stages: first, we develop equations for the equilibrium condition; then, we extend the treatment to include nonequilibrium effects that arise during cooling to room temperature prior to the FTIR spectroscopic measurement. The cavities are assumed to have a single diameter and to contain equal amounts of H. In describing equilibrium we take the solution condition as the reference state as a matter of convenience. Further, as discussed in Sec. III B, we assume that the nonconfigurational part of the entropy of a H atom on the surface is not very different from that of a H atom in solution. With this approximation, the concentration in solution, C_s, is related to the depth-integrated areal density of internally chemisorbed H, $\Lambda_{Ge\text{-}H}$, by

$$C_s \cong \{\Lambda_{Ge\text{-}H}/[\Lambda_{Ge\text{-}}-\Lambda_{Ge\text{-}H}]\}\exp(-Q_1/kT) \ . \quad (8)$$

Here $\Lambda_{Ge\text{-}}$ is the total, depth-integrated areal density of cavity-wall chemisorption sites and has the value given in Table I, and Q_1 is the energy to promote a H atom from chemisorption to solution and is related to the Ge-H bond energy E_B by Eq. (5). Since an assumption of constant entropy is inappropriate for the transition between the molecular gas and solution, we employ the experimentally determined relation

$$C_s = C_{so} P^{1/2} \exp(-Q_2/kT) \ , \quad (9)$$

where C_{so} and Q_2 are as defined previously and have the values given in Table I, and P is the H_2 pressure in the cavity. [For this calculation we use the pressure instead of the fugacity in Eq. (9) because it considerably simplifies the mathematics, and the resulting error is inconsequential. For example, at a temperature of 1000 K and a pressure of 10 MPa, which typify our experimental conditions, the fugacity is calculated from the equation of state[20] to be only 4% greater than the pressure.] The condition for equilibrium between chemisorption and molecular gas is then obtained by equating the right-hand sides of Eqs. (8) and (9).

We now consider the change in $\Lambda_{Ge\text{-}H}$, the quantity sensed by FTIR spectroscopy, during cooling to room temperature before the measurement is made. This change is governed by two opposing processes, namely recombinative desorption of H from the wall into the cavity void and dissociative adsorption of H_2 onto the wall, and it is given by

$$[d/dt]\Lambda_{\text{Ge-H}}=-[\nu_D/\Lambda_{\text{Ge-}}]\exp(-E_D/kT)[\Lambda_{\text{Ge-H}}]^2 + [\nu_D/\Lambda_{\text{Ge-}}][kT/2][C_{so}^2/\Lambda_V]\exp[-(E_D+E_R-2E_B)/kT][\Lambda_{\text{Ge-}}-\Lambda_{\text{Ge-H}}]^2[\Lambda_H-\Lambda_{\text{Ge-H}}] , \quad (10)$$

where ν_D is an attempt frequency for desorption, Λ_V is the depth-integrated cavity volume per unit sample area, Λ_H is the total areal density of H within the sample, and the various energies are as defined for Eq. (1). The first term on the right-hand side of Eq. (10) has the usual form for desorption with second-order kinetics,[6] while the second term is derived by requiring that the equilibrium condition given by Eqs. (8) and (9) is recovered when $[d/dt]\Lambda_{\text{Ge-H}}=0$. It may be noted that, from Eq. (1), the combination of energies appearing in the second term as the argument of the exponent is equal to E_A, the activation energy for adsorption.

Equation (10) assumes second-order desorption kinetics, which implies that the H occupation of chemisorption sites is random, as opposed to pairing or other clustering behavior. Random chemisorption is also implicit in Eq. (8). There is substantial justification for this assumption, since observations on both Si and Ge show second-order desorption from the (111) surface,[6,7,9] and detailed microstructural studies of cavities in Si indicate that the (111) surface is predominant.[26,27] In the case of the (100) surfaces of Si and Ge, however, first-order desorption is observed,[6,8,10] presumably reflecting pairing of the H. Since the cited microstructural studies of Si show a significant component of (100) cavity facets, this may represent an appreciable source of error for Eqs. (8) and (10). Fortunately, the quantity to be determined using Eq. (10), E_B, appears as the argument of an exponent, making its evaluation less sensitive to detailed assumptions regarding kinetics. A further possible complication is that the energies E_B and E_D may depend on the surface orientation. We believe, however, that in the case of monohydride bonding this difference is sufficiently small to be inconsequential for the objectives of the present paper. For Si, values of E_D for the (111) and (100) surfaces reported in the same paper[6] differ by less than 0.2 eV. Moreover, on physical grounds, the Ge-H bond energy is expected to be determined predominantly by the bonding of the Ge atom attached to the H, and this is $\text{Ge}_3\equiv\text{Ge}$—H for the monohydride states on both surfaces.

Equation (10), which describes both equilibrium and nonequilibrium conditions, allows us now to estimate the Ge-H surface-bond dissociation energy E_B from the FTIR spectroscopic data. We begin by using these data to calculate the fraction of the total contained H that exists as IR-sensitive, internal-surface Ge-H after annealing at 823 K or above, where the equilibrium partition between molecular gas and chemisorption is believed to be established. The average of the three spectral areas given in Fig. 4 for this temperature range is 0.23 cm^{-1}. By comparison, the average of the three areas listed in Fig. 5, where all of the H is assumed to exist as Ge-H at defects and hence be IR sensitive, is 4.02 cm^{-1}. From the ratio of these quantities we infer that the internally chemisorbed fraction is approximately 0.06, corresponding to 6 H/nm^2. We estimate the uncertainty in this quantity to be approximately a factor of 2, predominately due to the possibility of a difference in IR-absorption strength between the Ge-H centers on the cavity walls and those associated with defects which we use as a reference. Since the areal density of available chemisorption sites was estimated from TEM to be 26 nm^{-2}, about one site in four is occupied.

The next step is to solve Eq. (10) with the desired Ge-H bond energy as an adjustable parameter. All quantities other than E_B are independently evaluated as summarized in Table I, and during cooling the elevated temperature is taken to decay exponentially to 378 K with a time constant of 170 s as determined experimentally. The desorption attempt frequency ν_D is set equal to 10^{16} s^{-1}, a midrange value for this parameter whose reported magnitude ranges over two decades or more depending on surface orientation and investigator (see, e.g., Refs. 6–9 and citations therein.) Figure 7 shows computational results for $E_B=1.9$ eV and an initial temperature of 823 K. Here the equilibrium between gas and chemisorption is seen to persist until about 550 K, where desorption stops and the partition becomes frozen. The final areal density of Ge-H from Fig. 7 is 5.5 nm^{-2}, very close to the experimentally derived value of 6 nm^{-2}. In comparison, when E_B is assigned values of 1.8 and 2.0 eV, the respective calculated areal densities are 1.2 and 16.1 nm^{-2}, in strong disagreement with experiment. These calculated values are fortunately quite insensitive to the precise details of the desorption process; for example, when ν_D is increased by a factor of 100 and E_B is held at 1.9 eV, the final areal

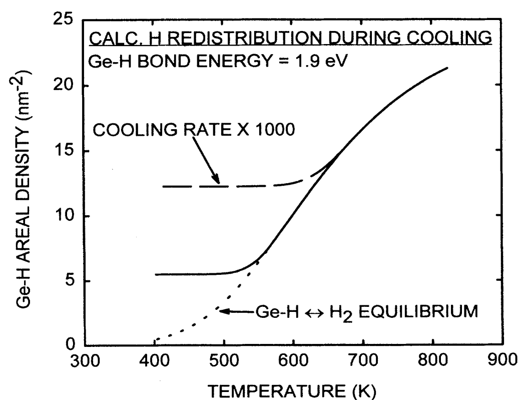

FIG. 7. Calculated variation of the amount of Ge-H on cavity walls during cooling from 873 K. The total areal density of H is 100 nm^{-2}. The dashed line represents the equilibrium between chemisorption and molecular gas at lower temperatures where the equilibrium is no longer maintained.

density of chemisorbed H decreases only from 5.7 to 2.7 nm^{-2}. One of the principal reasons for this insensitivity is the relatively modest energy difference between the competing chemisorbed state and molecular gas, about 0.4 eV per atom, as a consequence of which the temperature where the transfer between states stops need not be determined with great accuracy. We conclude from these considerations that the dissociation energy for the Ge-H surface monohydride bond is 1.9 eV, with an estimated uncertainty of ± 0.2 eV. This is consistent with the upper bound of 2.0 eV extracted from the thermal-release data in Fig. 2.

The above analysis can be subjected to two consistency checks. First, since during cooling the gas and chemisorbed state are predicted to remain in equilibrium until about 550 K, the areal density of Ge-H observed by IR spectroscopy should be the same for the three anneal temperatures 823, 848, and 873 K. This expectation is seen in Fig. 4 to be fulfilled. Second, when the total amount of implanted H is reduced, the areal density of Ge-H should also decrease, but less than proportionally. In particular, if the calculation of Fig. 7 is repeated for a total H content of 10 rather than 100 atoms/nm^2, the predicted areal density of wall Ge-H decreases from 5.7 to 2.2 nm^{-2}, a reduction of a factor of 2.6. Here the comparison with relevant experimental data, which are given in Fig. 6, is imprecise because of the weaker signal, the frequency dependence of the background absorption, and the not-easily-resolved tail extending from the principal peaks to lower frequencies. For the calculation we use the spectra obtained after anneals at 673, 723, and 773 K, respectively, because their appearance suggests that the gas-chemisorption equilibration of interest has been reached, and that significant loss of H from the sample has not occurred. The integration of area is carried out in the same way as in Fig. 4, and over the same frequency range. The average of the three absorption areas is 0.10 cm^{-1} with an estimated uncertainty of a factor of 1.5. This is smaller by a factor of 2.3 than the area obtained at the higher H dose, consistent with the model prediction of a factor of 2.6.

The predicted changes during cooling that are represented in Fig. 7 lead one to consider quenching more rapidly, which could in principle freeze in any equilibrium state of interest and thereby (1) avoid the cooling complications embodied in Eq. (10), and (2) permit the temperature dependence of the equilibrium condition to be observed. This approach is complicated, however, by the fact that the rate of desorption leading to equilibrium varies with temperature very rapidly and also much more rapidly than the partition of H between states, the respective activation energies being $E_D = 1.82$ eV and $E_R/2 - E_B = 0.36$ eV. As a result, to immobilize states over a significant temperature range would require access to annealing times extending over many orders of magnitude, and the resulting change in Ge-H areal density would be comparatively small. These points are illustrated by a second calculation depicted in Fig. 7, where the cooling rate was increased by 1000 times. This much more rapid quench is seen to increase the temperature at which evolution stops by only about 100 K, causing the amount of Ge-H to increase by only a factor of 2. We qualitatively confirmed this property by moving the sample directly from the furnace into a liquid-N_2 bath, thereby reducing the cooling time by at least an order of magnitude. This produced no significant change in the strength of the IR absorption from Ge-H. Further experiments of this kind may well prove illuminating, however, if sufficiently wide ranges of annealing time are accessed by methods such as rapid thermal annealing and electron-beam annealing. In particular, observation of the temperature dependence of the equilibrium condition that is predicted in Fig. 7 would provide important confirmation of the interpretation of H behavior presented here.

IV. DISCUSSION AND IMPLICATIONS

By examining the interaction of H with internal surfaces in Ge, we have determined that the dissociation energy of the Ge-H surface monohydride bond is $E_B = 1.9 \pm 0.2$ eV. Since this determination was based on observations of equilibrium between H_2 gas and the chemisorbed state, the resulting energy should include the effects of whatever lattice relaxations and reconstructions occur after the H atom is removed. Further, given the experimental conditions and the approximations made in data analysis, E_B is more accurately regarded as the enthalpy change associated with bond dissociation in the temperature range of our experiments, rather than the change in free energy (or equivalently the enthalpy) for dissociation at 0 K. Since this difference is unlikely to amount to more than a few tenths of an eV, the distinction is not an important one for many purposes. We also note that a more precise evaluation of the bond-dissociation enthalpy from our data would be possible if the change in the nonconfigurational, vibrational part of the entropy were independently measured or calculated. To our knowledge such measurements are unavailable, however, and the theoretical problem may not be trivial given the possibility of relaxations and reconstructions accompanying the removal of the H. Finally, based on considerations enumerated in Sec. III, E_B is expected to have little dependence on the surface orientation.

The above bond energy for Ge, coupled with our earlier finding of $E_B = 2.6 \pm 0.1$ eV for Si,[11,12] has several implications. Among the simplest is the relative stability of the chemisorbed states and molecular gas: since the dissociation energy per atom for H_2 is $E_R/2 = 2.26$ eV, one has, in order of increasing state energy, (1) H chemisorbed on Si, (2) H_2 gas, and (3) H chemisorbed on Ge. Further, by using the bond energies E_B from the present studies in Eq. (1) together with the published desorption activation energies of $E_D = 1.8$ eV for Ge,[10] and about 2.5 eV for Si (summary in Ref. 11), the activation energies for dissociative adsorption can be obtained. This calculation yields $E_A = 2.5$ eV for Ge and 1.8 eV for Si. These large values are consistent with the generally observed difficulty of dissociatively chemisorbing H_2 onto Ge and Si (see, e.g., Ref. 28). While the kinetic energy of H_2 molecules desorbing from the (111) Si surface has recently been reported to be $\sim kT$ (Ref. 29), which is much small-

er than our value of E_A, this does not necessarily conflict with the present results since the H_2 molecule formed may undergo substantial thermalization before its release from the surface. Moreover, an appreciable fraction of the decrease in system energy following the desorption saddle point may occur through structural rearrangements after the molecule has left the surface, and this component would not contribute to the kinetic energy of the molecule.

The Ge-H and Si-H surface-bond dissociation energies obtained in our studies are significantly smaller than those reported for the removal of a H atom from gaseous GeH_4 and SiH_4, the latter values being 3.7 and 3.9 eV, respectively.[25,30] Our value of 2.6 eV for the bare Si surface, however, is essentially identical to the measured activation energy for detachment of H atoms from isolated Si dangling bonds on the Si side of the Si-SiO_2 interface, 2.56±0.06 eV (Ref. 31). These differences may reflect the influence on the H-semiconductor bond of the other bonding reactions undergone by the same semiconductor atom, as a result of which H binds less strongly to $Ge_3\equiv$Ge— and $Si_3\equiv$Si— than to $H_3\equiv$Ge— and $H_3\equiv$Si—.

V. CONCLUSION

We have examined the interaction of H with cavities in Ge using nuclear-reaction analysis and FTIR vibrational spectroscopy, and by analyzing the results we have achieved an experimental determination of the Ge-H surface-monohydride-bond dissociation energy, the value being 1.9±0.2 eV. This work follows a similar study in Si, where the Si-H surface-bond energy was determined to be 2.6±0.1 eV. These bond strengths are substantially smaller than those reported for molecular silane and germane, possibly reflecting a pronounced interaction among the four bonds formed by a Ge or Si atom. The results illuminate mechanisms of H chemisorption and desorption on semiconductors and also provide a basis for more quantitative description of technologically important chemical vapor deposition and H passivation of Si-Ge alloys. Moreover, they reveal that the chemisorbed state of H on Ge is energetically less stable than H_2 gas, whereas the chemisorbed state on Si is more stable.

ACKNOWLEDGMENTS

The authors acknowledge valuable discussions with W. R. Wampler. Much of the experimental work was carried out by D. M. Bishop and M. P. Moran. This study was performed under the auspices of the U. S. Department of Energy and funded by its Office of Basic Energy Sciences, Division of Materials Sciences, under Contract No. DE-AC04-94AL85000.

[1]G. S. Higashi, Y. Chabal, G. W. Trucks, and K. Raghavachari, Appl. Phys. Lett. **56**, 656 (1990).
[2]N. M. Russell and W. B. Breiland, J. Appl. Phys. **73**, 3525 (1993).
[3]J. J. Boland, Phys. Rev. Lett. **65**, 3325 (1990).
[4]J. J. Boland, Surf. Sci. **244**, 1 (1991).
[5]T. Klitsner and J. S. Nelson, Phys. Rev. Lett. **67**, 3800 (1991).
[6]M. L. Wise, B. G. Koehler, P. Gupta, P. A. Coon, and S. M. George, Surf. Sci. **258**, 166 (1991).
[7]G. A. Reider, U. Höfer, and T. F. Heinz, J. Chem. Phys. **94**, 4080 (1991).
[8]U. Höfer, L. Li, and T. F. Heinz, Phys. Rev. B **45**, 9485 (1992).
[9]L. Surnev and M. Tikhov, Surf. Sci. **138**, 40 (1984).
[10]M. P. D'Evelyn, S. M. Cohen, E. Rouchouze, and Y. L. Yang, J. Chem. Phys. **98**, 3560 (1993).
[11]S. M. Myers, D. M. Follstaedt, H. J. Stein, and W. R. Wampler, Phys. Rev. B **47**, 13 380 (1993).
[12]W. R. Wampler, S. M. Myers, and D. M. Follstaedt, Phys. Rev. B **48**, 4492 (1993).
[13]H. J. Stein, S. M. Myers, and D. M. Follstaedt, J. Appl. Phys. **73**, 2755 (1993).
[14]J. F. Ziegler, J. P. Biersack, and U. Littmark, *The Stopping and Range of Ions in Solids* (Pergamon, New York, 1985); J. F. Ziegler (private communication).
[15]A. Van Wieringen and N. Warmoltz, Physica **22**, 849 (1956).
[16]J. W. Mayer, L. Eriksson, and J. A. Davies, *Ion Implantation in Semiconductors: Silicon and Germanium* (Academic, New York, 1970), p. 120.
[17]C. G. Van de Walle, Phys. Rev. B **49**, 4579 (1994).
[18]M. W. Chase, Jr., C. A. Davies, J. R. Downey, Jr., D. J. Frurip, R. A. McDonald, and A. N. Syverud, J. Phys. Chem. Ref. Data **14**, Suppl. 1, 1260 (1985).
[19]R. C. Frank and J. E. Thomas, Jr., J. Phys. Chem. Solids **16**, 144 (1960).
[20]H. Hemmes, A. Driessen, and R. Griessen, J. Phys. C **19**, 3571 (1986).
[21]H. J. Stein, J. Electron. Mater. **4**, 159 (1975).
[22]J. W. Corbett, P. Deák, U. V. Desnica, and S. J. Pearton, in *Hydrogen in Semiconductors,* edited by J. I. Pankove and N. M. Johnson (Academic, New York, 1991), pp. 49–64.
[23]J. E. Crowell and G. Lu, J. Electron Spectrosc. Relat. Phenom. **54-55**, 1045 (1990).
[24]Y. J. Chabal, Surf. Sci. **168**, 594 (1986).
[25]R. C. Binning, Jr. and L. A. Curtiss, J. Chem. Phys. **92**, 1860 (1990), and citations therein.
[26]D. M. Follstaedt, Appl. Phys. Lett. **62**, 1116 (1993).
[27]D. J. Eaglesham, A. E. White, L. C. Feldman, N. Moriya, and D. C. Jacobson, Phys. Rev. Lett. **70**, 1643 (1993).
[28]W. Ho (unpublished) as cited in Ref. 29.
[29]K. W. Kolasinski, W. Nessler, A. de Meijere, and E. Hasselbrink, Phys. Rev. Lett. **72**, 1356 (1994).
[30]R. Walsh, Acc. Chem. Res. **14**, 246 (1981).
[31]K. L. Brower, Phys. Rev. B **42**, 3444 (1990).

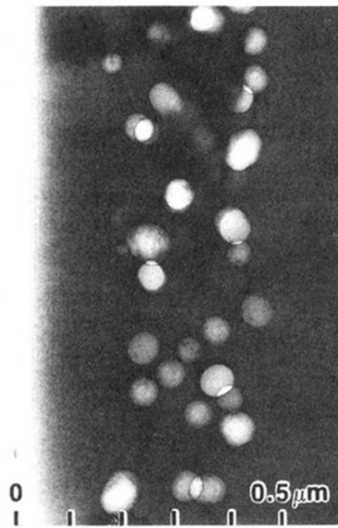

FIG. 1. Cross-section bright-field TEM micrograph of Ge that was ion implanted with 1000 He/nm^2 at 50 keV and then vacuum annealed for 30 min at 973 K. The orientation is [$11\bar{2}$], and the imaging was performed at a slight underfocus to enhance the contrast of open volumes.